World Academy of Science, Engineering and Technology
International Journal of Mechanical and Mechatronics Engineering
Vol:3, No:8, 2009

Optimization of Three-dimensional Electrical Performance in a Solid Oxide Fuel Cell Stack by a Neural Network

Shih-Bin Wang, Ping Yuan, Syu-Fang Liu, Ming-Jun Kuo

***Abstract*—**By the application of an improved back-propagation neural network (BPNN), a model of current densities for a solid oxide fuel cell (SOFC) with 10 layers is established in this study. To build the learning data of BPNN, Taguchi orthogonal array is applied to arrange the conditions of operating parameters, which totally 7 factors act as the inputs of BPNN. Also, the average current densities achieved by numerical method acts as the outputs of BPNN. Comparing with the direct solution, the learning errors for all learning data are smaller than 0.117%, and the predicting errors for 27 forecasting cases are less than 0.231%. The results show that the presented model effectively builds a mathematical algorithm to predict performance of a SOFC stack immediately in real time.

Also, the calculating algorithms are applied to proceed with the optimization of the average current density for a SOFC stack. The operating performance window of a SOFC stack is found to be between 41137.11 and 53907.89. Furthermore, an inverse predicting model of operating parameters of a SOFC stack is developed here by the calculating algorithms of the improved BPNN, which is proved to effectively predict operating parameters to achieve a desired performance output of a SOFC stack.

***Keywords*—**a SOFC stack, BPNN, inverse predicting model of operating parameters, optimization of the average current density

I. INTRODUCTION

Including two electrodes of anode and cathode, as well as one solid electrolyte between the anode and cathode, a solid oxide fuel cell (SOFC) delivers oxygen ions from cathode to anode. Methane and ethanol serve as the fuel, whose operating temperature is very high about 600-1000°C. Many studies had been investigated in the performance simulation under different conditions recently; such the effects of fuel rate, inlet temperature, operation pressure, cell size, etc. on the temperature and current density distribution. Yakabe et al. [1] modeled an anode-supported planar SOFC unit with double channels of counter-flow pattern. Their results indicated that the water shift reaction could effectively reduce the concentration polarization. Later, Yakabe et al. [2] simulated a three-dimensional model for a unit of planar SOFC, in the considerations of internal or external steam reforming, water shift reaction, and diffusion of gases with co-flow or counter-flow pattern. Recknagle et al. [3] also simulated a three-dimensional unit of SOFC with three kinds of flow patterns, i.e. co-flow, counter-flow, and cross-flow. Their results showed that the pattern of the co-flow had the most uniform temperature distribution and the smallest thermal gradients. Beale, et al. [4] investigated three different approaches in numerical methods for solving a unit and ten-stack SOFC in cross-flow, which results indicated that the direct numerical method is the most accurate method for a single cell, and the simpler approaches have the potential to supplant or complement the direct numerical method in the analysis of fuel cell stacks. The study of Iwata et al. [5] investigated the effects of gas re-circulation ratio, operating pressure and physical properties on current and temperature distributions by establishing a numerical program to estimate the temperature and current density profiles of a planar-type SOFC unit with co-flow, counter-flow, and cross-flow.

Also, coupling electrochemical kinetics with fluid dynamics, Huang et al. [6] developed a multi-physics model to evaluate the transport phenomena in a mono-block-layer SOFC. Because the spatial variation of the catholic and anodic surface over-potential is considered locally, their model improves the prediction of the local current density distribution. Janardhanan et al. [7] offered a performance analysis of a planar solid oxide fuel cell under direct internal reforming conditions to study the influences of various operating parameters on cell performance. Their results suggested that the efficiency of the fuel cell is higher for pre-formed fuel compared with non-reformed fuel. Araki et al. [8] presented a power generation system consisting of two SOFCs at different operating temperatures and in the serial connection. Their results showed that the power generation efficiency of the two-stage SOFC is somewhat higher than that of SOFC using only a high-temperature.

However, few reports have investigated the effects of non-uniform inlet flow on fuel cell temperature and current density. Hirata and Hori [9] presented a numerical method to

S. B. Wang is with the Department of Mechanical Engineering, Lee Ming Institute of Technology, 2-2, Lee Zhuan Road, Taishan, Taipei, Taiwan, ROC (corresponding author to provide phone: 886-2-29097811 ext: 1550; fax: 886-2-29095888; e-mail: wsb@mail.lit.edu.tw).

Ping Yuan is with the Department of Mechanical Engineering, Lee Ming Institute of Technology, Taishan, Taipei, Taiwan, ROC (e-mail: pyuan@mail.lit.edu.tw).

S. F. Liu is with the Department of Mechanical Engineering, Lee Ming Institute of Technology, Taishan, Taipei, Taiwan, ROC (e-mail: sfl@mail.lit.edu.tw).

M. J. Kuo is with the Department of Mechanical Engineering, Lee Ming Institute of Technology, Taishan, Taipei, Taiwan, ROC (e-mail: mjkuo@mail.lit.edu.tw).

discuss the relationships between planar and stacking direction gas flow uniformities, and cell performance in a co-flow type fuel cell. Liu et al. [10] as well as Yuan and Liu [11] developed a reliable numerical method to examine the effect of inlet flow maldistribution in the transverse direction on the thermal and electrical performance of a MCFC and SOFC unit with cross-flow configuration. Their results showed that the non-uniform inlet flow has only slightly effects on the average temperature and average current density, but induces significantly the non-uniformities of temperature and current density for most maldistribution patterns. The non-uniform gas flow rate in each stack is very severe because of the gas manifold. Some research [12], [13] and [14] identified an obvious maldistribution of the gas flow rate in the stacking direction of a SOFC stack.

Also, Yuan [15] investigated the non-uniform effect of gas flow rate on the thermal and electrical performance of a SOFC stack, considering a uniform profile and a progressively increasing profile in the stacking direction with two boundary conditions, adiabatic and constant temperature, on the top and bottom faces of a SOFC stack. His results show that the non-uniform inlet flow rate of the fuel dominates the current density distribution, and the air dominates the temperature field of a SOFC. Also, the power at the constant boundary temperature condition can elevate 3% more than that at the adiabatic boundary condition. Although the non-uniform effect on the electrical performance of each stack is apparently realized, the optimal conditions in consideration of all non-uniform inlet flow rates and parameters as well as their importance are still difficult to obtain by the numerical method.

Instead of the numerical method, neural network architecture has currently become more and more important as an effective learning technique in the field of pattern recognition since neural networks have strong abilities to learn, to self-organize information, and need only few specific requirements and prior assumptions for modeling. These advantages have attracted interest in research on SOFC performance prediction. Arriagada et al. [16] developed a novel modeling tool for evaluation of solid oxide fuel cell performance by an artificial neural network at different operational parameters of the SOFC, such as gas flows, operational voltages, current density, etc.

Based on the analyses [15], global performance for a solid oxide fuel cell (SOFC) stack will proceed further with the development of a rapid performance prediction scheme in this study. Usually, it needs a lot of computer calculating time to obtain the direct solutions of temperature and current density filed by the numerical method. Therefore, a rapid calculation scheme for predicting the average temperature and current density in each layer of a SOFC stack by the application of back propagation neural network (BPNN) will be developed. The algorithm developed by the BPNN will provide a rapid prediction of current density so as to complete dynamic control when the mole fraction of species and molar flow rate in inlet is considered to be changeable.

The researching method first utilizes Taguchi's orthogonal array to arrange the inputs of BPNN with different factors and levels, and the direct solutions of average current densities of each layer of a SOFC stack for every case derived by the numerical method [15] serve as the outputs of BPNN. Thus, the important priority of factors is firstly decided by the analysis of variance (ANOVA), and then an improved Back-Propagation Neural Network is utilized to learn the learning data and build a model of performance for a SOFC stack. Thus, the mathematical algorithms are applied to proceed with the optimization of the average current density. Finally, by the calculating algorithms of the improved BPNN, an inverse predicting model of operating parameters to achieve a desired performance output of a SOFC stack will be developed.

II. Description of the Theory

A solid oxide fuel cell stack investigated here is formed by connecting 10 unit cells as shown in Fig. 1. The unit cell from top to bottom includes the interconnector with the flow channels, fuel, anode, electrolyte, cathode and air. The size of the unit cell is 0.2 m × 0.2 m in the x–y plane, and the fuel and the air flows along the interconnecting channels as well as along the x and y direction. The thicknesses of the unit cell, interconnector and interface between interconnector and cell are 0.6×10^{-3}m, 3×10^{-3} m, 1.8×10^{-3} m, respectively. In our previous investigation [15] suggested that the non-uniform inlet molar flow rate of the fuel in the stacking direction induces larger cell voltage variations. Therefore, a better operation for a SOFC is keeping constant inlet profile in fuel side here. Because this study plans to find the important factors of operation and the suitable operation conditions in a certain electrical performance, only a uniform profile in the fuel side and a uniform or progressively increasing profile in the air side are considered to construct two patterns of non-uniform inlet air flow. Fig. 2 shows the whole SOFC stack with two inlet flow distributions.

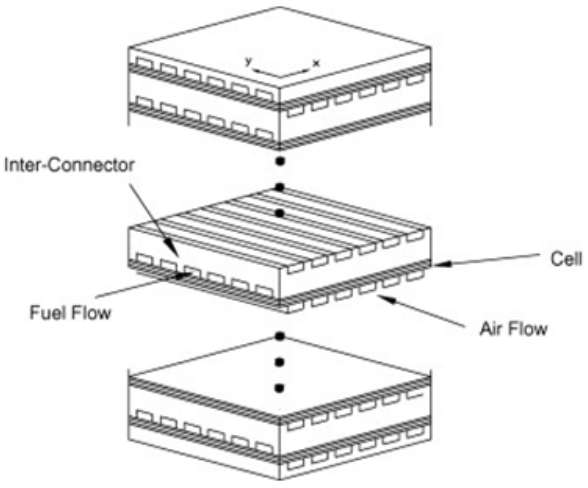

Fig. 1. Schematic diagram of a unit solid oxide fuel cell stack with cross-flow configuration.

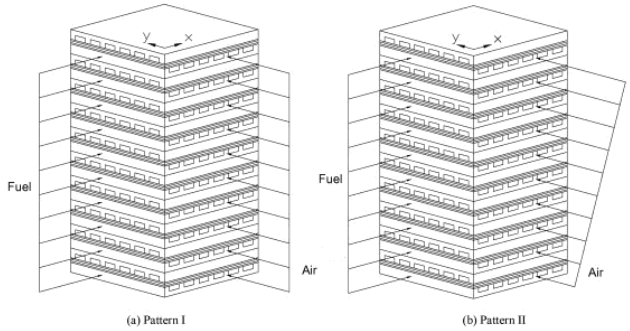

Fig. 2. Two inlet flow patterns in an SOFC stack.

This study uses the numerical results in literature [15] to obtain the learning data of BPNN, where FORTRAN code was applied to solve the mass equations, energy equations, and electrochemistry equations. The composition of fuel includes hydrogen (H_2), nitrogen (N_2), carbon dioxide (CO_2), carbon monoxide (CO) and water (H_2O). The mass equations connect the molar flow rate change in the fuel and the air, and the species consumption linking the local current density. Moreover, the conservation of energy for the fuel, air, cell, and interconnector for each stack are taken into consideration.

The molar flow rate of the fuel and the air in each stack is different because of the non-uniform distribution of molar flow rates in the stacking direction. In this study, the non-uniform flow pattern in the stacking direction has a progressively increasing profile, so the molar flow rate of each stack can be expressed in terms of the stack number as follows:

$$n_{\mathrm{f}}^{k}=\bar{n}_{\mathrm{f}}\left(\frac{2d_{\mathrm{stack,f}}^{k}}{(n_{\mathrm{stack}}-1)}(k-1)+(1-d_{\mathrm{stack,f}}^{k})\right) \quad (1)$$

$$n_{\mathrm{a}}^{k}=\bar{n}_{\mathrm{a}}\left(\frac{2d_{\mathrm{stack,a}}^{k}}{(n_{\mathrm{stack}}-1)}(k-1)+(1-d_{\mathrm{stack,a}}^{k})\right) \quad (2)$$

,where $\overline{n}_f$ and $\overline{n}_a$ represents the mean flow rate of the fuel and the air in the SOFC stack, and the molar flow rate in each stack depends on the deviation in the stacking direction, d_{stack}, as well as the total number of cells, n_{stack}. The deviation in the stacking direction is the ratio of the variation of flow rate to the mean flow rate; its value may be positive or zero, representing the progressively increasing profile and uniform profile, respectively.

In the numerical analysis [15], the voltage loss caused by electrolyte ohmic polarization, electrode activation polarization and concentration polarization are considered. Therefore, the cell voltage equals the Nernst voltage minus the polarization voltages (ohmic, activation and concentration) in the anode, as follows:

$$V^{k}=E^{k}-V_{\mathrm{ohm}}^{k}-V_{\mathrm{act}}^{k}-V_{\mathrm{con}}^{k} \quad (3)$$

$$V_{\mathrm{ohm}}^{k}=i^{k}r \quad (4)$$

$$V_{\mathrm{act}}^{k}=\frac{RT_{\mathrm{c}}^{k}}{2F}\sinh^{-1}\left(\frac{i^{k}}{2i_{0,\mathrm{anode}}}\right)+\frac{RT_{\mathrm{c}}^{k}}{2F}\sinh^{-1}\left(\frac{i^{k}}{2i_{0,\mathrm{cathode}}}\right) \quad (5)$$

$$V_{\mathrm{con}}^{k}=-\frac{RT_{\mathrm{c}}^{k}}{2F}\ln\left[\frac{1-(RT_{\mathrm{c}}^{k}/2F)(\delta_{\mathrm{anode}}/D_{\mathrm{anode}}p_{\mathrm{H_2}})i^{k}}{1+(RT_{\mathrm{c}}^{k}/2F)(\delta_{\mathrm{anode}}/D_{\mathrm{anode}}p_{\mathrm{H_2O}})i^{k}}\right] \quad (6)$$

Here r is 300×10^{-7} Ω m^{-2} [20], $i_{0,\mathrm{anode}}$ and $i_{0,\mathrm{cathode}}$ are 1290 and 970 A m^{-2} [21], respectively, δ_{anode} is 0.05 mm, and D_{anode} is 2×10^{-5} m s^{-1} [22]. The method of solving these governing equations in a SOFC unit has been developed in the author's previous research [20]. The numerical method by FORTRAN code uses mass and energy balance equations to solve the mole fraction of each species, as well as the temperatures of the fuel, air, cell, and interconnector. The solving method then calculates the current density from Eqs. (3) to (6), based on the assumption that the cell voltage is uniform over the cell reaction area.

III. Modeling by Back-Propagation Neural Network

The algorithm of the back propagation neural network (BPNN) can map the I/O relationship adequately and is readily suitable for multivariable systems. However, it inherits the major defect from gradient descent techniques that the set of selecting parameters usually minimizes the learning error only at some interval and not at the global interval. Therefore, Wang and Wu [23] integrated an error distribution function to improve the BPN network, which is proved to be useful to overcome local minimum problem effectively, so as to find the global minimum solution and greatly accelerate the convenience speed. Hence, the algorithm of the improved BPNN will be applied here to establish a rapid calculating scheme for predicting the average current densities in each layer of a SOFC stack.

An artificial BPNN usually has multi-layers. The input layer accepts the environmental information; the output layer carries information to the environment. The layers lying between the input and output layers are called the hidden layers. The basic unit — the neuron — acts as a "processing element". For an example shown in Fig. 3, the *j*th neuron in the nth layer has many inputs x_1^{n-1} which come from the neurons in the (n-1)th layer, but only a single output x_j^n that carries its signal to the neurons in the (n+1)th layer. An adjustable weight, W_{ij}^n, representing the connecting strength, lies between the *j*th input branch in the nth layer and the ith neuron in the (n-1)th layer. The basic function (net sum) of a neuron is to sum up its inputs and by means of the transfer function to produce an output. An internal threshold t is usually introduced and subtracted from the sum. Mathematically, the net sum net_j^n of the jth neuron in the nth layer can be expressed as

$$net_j^n=\sum_i W_{ij}^n x_i^{n-1}-t_j^n \quad (7)$$

Then the output value x_j^n can be calculated as

$$x_j^n=f(net_j^n)=\frac{\theta_j^n}{1+e^{-\beta_j^n net_j^n}} \quad (8)$$

, where $f(\ )$ is the transfer function. The sigmoid function is a type of the transfer function used most commonly. Rangwala [24] presented a new form of the sigmoid function adopted here

as eq.(8) in order to make the network respond to arbitrary input/output mapping, where sigmoid slope β regulates the size of the input zone beyond which the neuron output saturates as well as the steepness of the sigmoid curve. The maximum output θ controls the maximum output of one neuron.

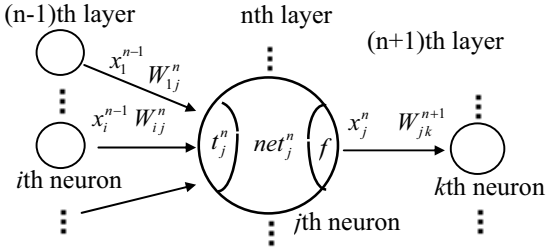

Fig. 3 Schematic diagram of a neuron model

In the back propagation learning scheme, the calculated outputs in the output layer, x_j^q, are compared with the desired outputs, d_j, to find the error, before the error signals are propagated backward through the network. The error function E can be defined as

$$E = \frac{1}{2}\sum_{j=1}^{p}(d_j - x_j^q)^2 \tag{9}$$

, where q is the total number of layers in the network and p the total number of the output neurons. The learning process is to adjust the learning parameters, W, t, β and θ, so that the error E can be minimized and the mapping between inputs and outputs can be realized. In order to accomplish this, gradient descent technique is applied to calculate the gradient of the error with respect to each learning parameter. Then the learning parameters are changed and adjusted in the direction of the steepest descent of the error. The training formulae to adjust W, t, β and θ can be written as

$$\Delta W_{ij}^n(T+1) = \eta\delta_j^n x_i^{n-1} + \gamma\cdot\Delta W_{ij}^n(T) \tag{10}$$

$$\Delta t_j^n(T+1) = -\eta\delta_j^n + \gamma\cdot\Delta t_j^n(T) \tag{11}$$

$$\Delta\beta_j^n(T+1) = \eta\zeta_j^n[x_j^n(1-x_j^n/\theta_j^n)net_j^n] + \gamma\cdot\Delta\beta_j^n(T) \tag{12}$$

$$\Delta\theta_j^n(T+1) = \eta\zeta_j^n(x_j^n/\theta_j^n) + \gamma\cdot\Delta\theta_j^n(T) \tag{13}$$

, where η is the learning rate, T is the iteration, and γ is the momentum factor, $0 \le \gamma < 1$. Also, the quantities δ_j^n, $\delta_j^n = -\partial E/\partial net_j^n$, and ζ_j^n, $\zeta_j^n = -\partial E/\partial x_j^n$, act like the errors that are propagated backward to the network. For the output layer, the quantity ζ_j^n is first decided by the difference of the desired outputs and the calculated outputs, and then the quantity δ_j^n can be expressed by the quantity ζ_j^n. Considering the output layer, δ_j^n and ζ_j^n can be written as bellows.

$$\zeta_j^n = (d_j - x_j^n) \tag{14}$$

$$\delta_j^n = \zeta_j^n x_j^n(1 - x_j^n/\theta_j^n)\beta_j^n \tag{15}$$

Secondly, these quantities of the output layer are propagated to the lower hidden layers. For the hidden layers, the quantities δ_j^n and ζ_j^n can be expressed as:

$$\zeta_j^n = \sum_k \delta_k^{n+1} W_{jk}^{n+1} \tag{16}$$

$$\delta_j^n = \zeta_j^n x_j^n(1 - x_j^n/\theta_j^n)\beta_j^n \tag{17}$$

IV. Optimization Using Improved BPNN

As mentioned above, the average current density for each layer in a SOFC stack can be obtained by the model developed by the improved BPNN. Usually, the power of a SOFC stack is illustrated by its current density. The larger of the sum of current densities for each layer means the greater performance for a SOFC stack. It attracts us great interest in where the best performance is and how the operating parameters of a SOFC stack are selected. Thus, an optimized design of operating parameters based on the performance of a SOFC stack is developed here, with a proper objective function F defined as

$$F = \sum_{j=1}^{p} c_j x_j^q \tag{18}$$

, where q is the total number of layers in the BPNN, p is the total number of the output neurons. Also, the weightings c_j for the average current density x_j^q of the jth layer in a SOFC stack are same here as value equal to 1. The optimized process is to adjust the operating parameters x_j^1, inputs for the input layer of the BPNN, so that the objective function can be maximized. In order to accomplish this, gradient descent technique is applied to calculate the gradient of the objective function with respect to each operating parameter. Then the operating parameters are changed and adjusted in the direction of the steepest descent of the objective function. The adjustment of the operating parameters can be expressed as

$$\Delta x_j^1(T+1) = \eta^*\frac{\partial F}{\partial x_j^1} + \gamma^*\cdot\Delta x_j^1(T) \tag{19}$$

, where η^* is the converging rate, $0 \le \eta^* < 1$, T is the iteration, and γ^* is the momentum factor, $0 \le \gamma^* < 1$. Also, all the operating parameters x_j^1 are constrained between their top and down levels.

In order to simplify the derivatives of F with respect to every operating parameter, following definitions are given

$$\frac{\partial F}{\partial net_j^n} = \mu_j^n \tag{20}$$

$$\frac{\partial F}{\partial x_j^n} = \nu_j^n \tag{21}$$

For output layer, the quantities ν_j^n and μ_j^n can be derived as

$$\nu_j^n = \frac{\partial F}{\partial x_j^n} = c_j \tag{22}$$

$$\mu_j^n = \frac{\partial F}{\partial net_j^n} = \frac{\partial F}{\partial x_j^n}\frac{\partial x_j^n}{\partial net_j^n} = \nu_j^n f'(net_j^n) = \nu_j^n x_j^n(1 - x_j^n/\theta_j^n)\beta_j^n \tag{23}$$

For hidden layers, the quantities ν_j^n and μ_j^n can be derived as

$$\frac{\partial F}{\partial x_j^n} = \sum_k \frac{\partial F}{\partial net_k^{n+1}}\frac{\partial net_k^{n+1}}{\partial x_j^n} \tag{24}$$

$$\nu_j^n = \sum_k \mu_k^{n+1} w_{jk}^{n+1} \tag{25}$$

$$\mu_j^n = \nu_j^n f'\left(net_j^n\right) = \nu_j^n x_j^n (1 - x_j^n / \theta_j^n)\beta_j^n \quad (26)$$

For input layer, the quantities ν_j^1 can be derived as

$$\nu_j^1 = \sum_k \mu_j^2 w_{jk}^2 \quad (27)$$

The quantities ν_j^n and μ_j^n are propagated backward, a calculating process similar to the above model developed by the improved BPNN. For the output layer, the quantity ν_j^n is first decided by the c_j, the weighting for the output average current density x_j^q of the jth layer in a SOFC stack, and then the quantity μ_j^n can be obtained by the quantity ν_j^n. The process of calculation is characterized by the adoption of the calculating algorithm of the BPNN from the output layer back propagated to the input layers. Thus, the adjustment of the operating parameter can be rewrote as

$$\Delta x_j^1(T+1) = \eta^* \nu_j^1 + \gamma^* \cdot \Delta x_j^1(T) \quad (28)$$

The scale of the performance, i.e. operating performance window, of a SOFC stack is desired in practical application, whose value is between the maximum F and minimum F. The Maximum F can be obtained as mentioned above. On the other hand, the minimum F can be achieved just by changing the opposite direction of the steepest descent of the objective function as the operating parameters are adjusted. Thus, the adjustment of the operating parameters for the minimum F can be expressed as

$$\Delta x_j^1(T+1) = -\eta^* \nu_j^1 + \gamma^* \cdot \Delta x_j^1(T) \quad (29)$$

V. Inverse Prediction of Operating Parameters by Using Improved BPNN

Sometimes the performance of a SOFC stack is requested to be maintained at or changed to a certain value in practical operation. An operator would prefer to efficiently realize the proper operating parameters to obtain the desired performance of a SOFC stack. Thus, the inverse prediction of operating parameters is developed here to achieve a desired performance of a SOFC stack. Once a desired performance output Q, limited in the operating performance window of a SOFC stack, is decided, the object function can be derived as the sum of square of the difference between a temporary performance and the desired Q value.

$$F = \left(\sum_{j=1}^{p} c_j x_j^q - Q\right)^2 \quad (30)$$

The desired performance is on the target when the object function has the minimum value, i.e. 0. Therefore, the optimized process is to adjust the operating parameters x_j^1 so that the objective function can be minimized. Similarly, gradient descent technique is applied to calculate the gradient of the objective function with respect to each operating parameter. Then the operating parameters are changed and adjusted in the reverse direction of the steepest descent of the objective function. The adjustment of the operating parameters can be expressed as

$$\Delta x_j^1(T+1) = -\eta^* \frac{\partial F}{\partial x_j^1} + \gamma^* \cdot \Delta x_j^1(T) \quad (31)$$

, where η^* is the converging rate, $0 \le \eta^* < 1$, T is the iteration, and γ^* is the momentum factor, $0 \le \gamma^* < 1$. Also, all the operating parameters x_j^1 are constrained between their top and down levels.

Similarly, the quantities ν_j^n and μ_j^n are defined as the above section, which calculating process are propagated backward by the application of BPNN. Differently, the quantity ν_j^n for the output layer is amended as

$$\nu_j^n = \frac{\partial F}{\partial x_j^n} = 2c_j\left(\sum_{j=1}^{p} c_j x_j^q - Q\right) \quad (32)$$

Also, the quantity μ_j^n is obtained by the quantity ν_j^n. The process of calculation applies the calculating algorithm of the BPNN from the output layer back propagated to the input layers. Thus, the adjustment of the operating parameter can be expressed as

$$\Delta x_j^1(T+1) = -\eta^* \nu_j^1 + \gamma^* \cdot \Delta x_j^1(T) \quad (33)$$

VI. Results and Discussions

6.1 The important priority of factors decided by Taguchi's method

For global approximation learning of the BPNN, it is very important that the training data uniformly cover the entire design space. Ideally, equal level for all factors and same distance between adjacent levels in a factor are preferred. This is easily achieved by a full factorial design. However, for many factors with many levels, the design points of training data are extremely huge, a result that make neural network approximation impossible. An alternative approach is to use randomly generated design space. The shortcoming with this approach is without guarantee that the design points will cover the entire space, especially as the number of factors is large. Furthermore, levels of factor may not distribute uniformly, so the learning processes would center on some special levels and large error occurs.

An ideal approach is to use Taguchi design [25]. This method is a partial factorial design which adopts orthogonal arrays to design training data, a characteristic that every level in all columns is self-balance as well as levels in any two columns are mutual-balanced. Also, this method can efficiently lower the design data with the consideration of the whole space and all levels. By utilization of Taguchi's method, moreover, the significance of factors can be assess by F-test cooperated with the analysis of variance (ANOVA). These advantages have attracted our interest in the adoption of this method to design the training data of the BPNN.

The array of the training data are carried out using a variety of factors and levels, as listed in Table 1. The unit of mole flow in both anode inlet and cathode inlet is mol s^{-1}. The other parameters and conditions are illustrated below. As air is provided for the cathode inlet, the molar fractions of X_{O_2}

and X_{N_2} in cathode inlet are thus fixed to 0.22 and 0.78, respectively. The inlet cell temperatures for both the fuel and the air are assigned at 898K. Heat transfer area per unit base area ($m^2\ m^{-2}$) is 1.0 for the interface between interconnector and air, interconnector and cell as well as interconnector and fuel. Also, heat transfer area per unit base area ($m^2\ m^{-2}$) is 0.5 for the interface between cell and air as well as cell and fuel. The conductivity ($W\ m^{-1}\ K^{-1}$) for the unit cell, interconnector and interface between interconnector and cell are 2, 13, 1, respectively. The ambient operation pressure is set to 1×10^5 Pa.

TABLE 1.
THE FACTORS AND LEVELS APPLIED IN $L_{50}(2^1\times5^{11})$

factor	description	symbo	Level 1	Level 1	Level 2	Level 3	Level 4	Level 5
A	Air flow deviation in the stacking direction	d_{stack}	1	1.5				
B	Mole flow rate in anode inlet	N_f	0.06	0.075	0.09	0.105	0.12	
C	Molar fraction H_2 in anode inlet	X_{H_2}	0.24	0.3	0.36	0.42	0.48	
D	Molar fraction CO_2 in anode inlet	X_{CO_2}	0.03	0.04	0.05	0.06	0.07	
E	Molar fraction H_2O in anode inlet	X_{H_2O}	0.03	0.04	0.05	0.06	0.07	
F	Molar fraction CO in anode inlet	X_{CO}	0.2	0.24	0.28	0.32	0.36	
G	Mole flow rate in cathode inlet	N_a	0.12	0.15	0.18	0.21	0.24	

TABLE 2.
THE DESIGN OF TRAINING DATA FOR ALL FACTORS AND LEVELS BY $L_{50}(2^1\times5^{11})$

Exp.	A	B	C	D	E	F	G	Ia1	Ia2	Ia3	Ia4	Ia5	Ia6	Ia7	Ia8	Ia9	Ia10	Ave.
1	1	1	1	1	1	1	1	4602.28	4650.64	4669.90	4677.02	4679.25	4679.10	4676.38	4668.03	4645.64	4589.95	4653.82
2	1	1	2	2	2	2	2	4627.48	4678.19	4697.31	4704.07	4706.09	4705.95	4703.45	4695.44	4672.95	4613.75	4680.47
3	1	1	3	3	3	3	3	4645.11	4697.39	4716.29	4722.71	4724.62	4724.49	4722.13	4714.44	4691.98	4630.25	4698.94
4	1	1	4	4	4	4	4	4658.16	4711.59	4730.27	4736.45	4738.25	4738.12	4735.90	4728.43	4706.03	4642.38	4712.56
5	1	1	5	5	5	5	5	4668.24	4722.50	4740.96	4746.92	4748.61	4748.49	4746.36	4739.12	4716.84	4651.68	4722.97
6	1	2	1	2	3	4	5	4330.87	4388.06	4406.71	4412.47	4414.01	4413.91	4411.98	4404.97	4382.35	4313.44	4387.88
7	1	2	2	3	4	5	1	4383.60	4437.12	4457.28	4464.31	4466.41	4466.28	4463.73	4455.46	4431.89	4369.83	4439.59
8	1	2	3	4	5	1	2	4435.49	4490.69	4510.37	4516.90	4518.76	4518.65	4516.36	4508.58	4485.30	4420.45	4492.16
9	1	2	4	5	1	2	3	5138.96	5190.07	5207.82	5213.55	5215.17	5215.06	5213.07	5206.18	5185.01	5124.40	5190.93
10	1	2	5	1	2	3	4	5076.95	5129.26	5147.00	5152.63	5154.20	5154.10	5152.14	5145.34	5124.01	5061.49	5129.71
11	1	3	1	3	5	2	4	4112.86	4172.65	4191.63	4197.29	4198.74	4198.65	4196.85	4190.01	4167.03	4095.18	4172.09
12	1	3	2	4	1	3	5	4880.57	4935.95	4953.35	4958.44	4959.77	4959.68	4958.04	4951.83	4930.69	4863.69	4935.20
13	1	3	3	5	2	4	1	4840.98	4893.77	4912.79	4919.09	4920.87	4920.76	4918.61	4911.19	4888.86	4827.39	4895.43
14	1	3	4	1	3	5	2	4825.91	4879.95	4898.69	4904.72	4906.39	4906.30	4904.24	4897.06	4874.83	4811.17	4880.93
15	1	3	5	2	4	1	3	4816.03	4871.45	4889.88	4895.54	4897.07	4896.98	4895.09	4888.28	4866.24	4800.26	4871.68
16	1	4	1	4	2	5	3	4516.82	4574.80	4593.13	4598.48	4599.85	4599.77	4598.09	4591.65	4569.65	4500.37	4574.26
17	1	4	2	5	3	1	4	4558.01	4616.69	4634.58	4639.67	4640.92	4640.85	4639.31	4633.15	4611.49	4540.72	4615.54
18	1	4	3	1	4	2	5	4585.81	4644.59	4662.31	4667.30	4668.55	4668.47	4666.93	4660.85	4639.28	4567.98	4643.21
19	1	4	4	2	5	3	1	4593.27	4649.68	4669.15	4675.27	4676.94	4676.84	4674.83	4667.61	4644.72	4578.73	4650.70
20	1	4	5	3	1	4	2	5304.75	5357.26	5374.72	5380.08	5381.51	5381.43	5379.68	5373.31	5352.53	5290.42	5357.57
21	1	5	1	5	4	3	2	4243.10	4303.63	4322.49	4327.82	4329.17	4329.10	4327.47	4321.10	4298.66	4226.76	4302.93
22	1	5	2	1	5	4	3	4322.32	4382.83	4401.24	4406.42	4407.68	4407.61	4406.08	4399.84	4377.71	4305.21	4381.69
23	1	5	3	2	1	5	4	5076.31	5132.51	5149.38	5154.03	5155.18	5155.11	5153.70	5148.07	5127.65	5059.81	5131.18
24	1	5	4	3	2	1	5	5020.80	5078.09	5094.73	5099.20	5100.26	5100.20	5098.88	5093.45	5073.17	5003.53	5076.23
25	1	5	5	4	3	2	1	4967.99	5023.60	5041.97	5047.49	5048.92	5048.84	5047.13	5040.62	5018.97	4953.70	5023.92
26	2	1	1	1	4	5	4	4176.25	4231.69	4251.33	4257.88	4259.80	4259.67	4257.28	4249.38	4225.87	4159.72	4232.89
27	2	1	2	2	5	1	5	4263.49	4319.59	4338.82	4345.09	4346.86	4346.73	4344.52	4336.93	4313.71	4246.24	4320.20
28	2	1	3	3	1	2	1	4952.89	4998.78	5017.31	5024.27	5026.48	5026.33	5023.65	5015.48	4993.92	4940.87	5002.00
29	2	1	4	4	2	3	2	4918.50	4967.16	4985.74	4992.40	4994.44	4994.30	4991.81	4983.91	4962.02	4905.04	4969.53
30	2	1	5	5	3	4	3	4893.95	4944.48	4963.02	4969.41	4971.30	4971.17	4968.83	4961.19	4939.17	4879.36	4946.19
31	2	2	1	2	1	3	3	4651.92	4705.25	4723.94	4730.07	4731.81	4731.70	4729.55	4722.22	4699.88	4636.51	4706.29
32	2	2	2	3	2	4	4	4668.03	4722.52	4740.98	4746.89	4748.52	4748.41	4746.39	4739.27	4717.03	4651.72	4722.98
33	2	2	3	4	3	5	5	4679.33	4734.67	4752.95	4758.65	4760.21	4760.11	4758.16	4751.25	4729.10	4662.31	4734.67
34	2	2	4	5	4	1	1	4673.05	4724.87	4744.52	4751.41	4753.46	4753.34	4750.84	4742.74	4719.72	4659.36	4727.33
35	2	2	5	1	5	2	2	4681.88	4734.99	4754.32	4760.87	4762.79	4762.66	4760.33	4752.53	4729.64	4667.13	4736.71
36	2	3	1	3	3	1	2	4343.84	4400.66	4420.21	4426.44	4428.14	4428.04	4425.95	4418.55	4395.32	4328.02	4401.52
37	2	3	2	4	4	2	3	4410.32	4467.85	4486.95	4492.83	4494.41	4494.32	4492.38	4485.32	4462.43	4393.69	4468.05
38	2	3	3	5	5	3	4	4457.89	4515.92	4534.62	4540.23	4541.71	4541.62	4539.79	4533.01	4510.45	4440.53	4515.58
39	2	3	4	1	1	4	5	5172.38	5225.81	5242.93	5248.09	5249.44	5249.36	5247.67	5241.41	5220.64	5155.94	5225.37
40	2	3	5	2	2	5	1	5090.24	5140.73	5159.37	5165.69	5167.52	5167.42	5165.21	5157.76	5135.86	5076.86	5142.67
41	2	4	1	4	5	4	1	4115.68	4174.65	4194.81	4201.14	4202.84	4202.75	4200.71	4193.25	4169.45	4100.15	4175.54
42	2	4	2	5	1	5	2	4894.30	4949.11	4967.36	4972.90	4974.38	4974.30	4972.50	4965.90	4944.18	4879.08	4949.40
43	2	4	3	1	2	1	3	4866.51	4922.41	4940.40	4945.74	4947.13	4947.06	4945.35	4938.94	4917.35	4850.34	4922.12
44	2	4	4	2	3	2	4	4847.83	4904.60	4922.38	4927.52	4928.83	4928.76	4927.15	4920.93	4899.45	4830.89	4903.83
45	2	4	5	3	4	3	5	4834.31	4891.74	4909.23	4914.19	4915.42	4915.36	4913.83	4907.79	4886.51	4816.71	4890.51
46	2	5	1	5	2	2	5	4535.56	4595.13	4612.37	4617.02	4618.12	4618.06	4616.71	4611.07	4590.06	4517.43	4593.15
47	2	5	2	1	3	3	1	4559.75	4617.21	4636.34	4642.15	4643.67	4643.60	4641.78	4634.93	4612.35	4544.60	4617.64
48	2	5	3	2	4	4	2	4588.80	4647.17	4665.77	4671.23	4672.61	4672.55	4670.88	4664.39	4642.21	4572.65	4646.83
49	2	5	4	3	5	5	3	4610.26	4669.25	4687.39	4692.53	4693.80	4693.73	4692.19	4686.02	4664.21	4593.30	4668.27
50	2	5	5	4	1	1	4	5328.33	5383.24	5399.78	5404.37	5405.49	5405.44	5404.07	5398.53	5378.48	5311.97	5381.97

Therefore, the input arrays of the training data in the BPNN are obtained by the Taguchi's orthogonal array $L_{50}(2^1\times5^{11})$, whose columns of the array from 1 to 7 are applied. The direct solutions of temperature and current density for each layer of a SOFC stack obtained by the previous numerical method [15] serve as the learning data. Thus, a total of 50 training data for the learning of the network are completed as listed in Table 2.

By the analysis of mean (ANOM), the response table is also listed in Table 3, where the rank is determined based on the average current density of a SOFC stack. Fig.4 plots the response graph. The effects of all control factors are determined by the analysis of variance (ANOVA), where F-test are executed to assess if control factors are significant. Table 4 lists the ANOVA, where the F-ratios, the percentage contributions for each process variable were calculated. The ranks in Table 4 were decided due to the value of F-ratios.

The Taguchi method for quality analysis is to achieve the evaluation of the optimal combination of working parameters. The optimal selected levels for every factor are decided according to their ranks. The obtained ranks of ANOVA in Table 4 are equal to those of the response table in Table 3. The significance of all factors in order is X_{H_2}, X_{H_2O}, N_f, N_a, respectively.

TABLE 3.
THE RESPONSE TABLE

	A	B	C	D	E	F	G
Level1	4744.86	4693.96	4420.05	4742.41	5053.37	4746.26	4732.86
Level2	4744.05	4726.82	4613.08	4744.17	4870.66	4741.44	4741.80
Level3		4750.85	4768.21	4742.97	4721.11	4741.70	4742.84
Level4		4768.27	4900.57	4746.79	4593.56	4745.20	4751.83
Level5		4782.38	5020.39	4745.94	4483.59	4747.68	4752.94
Effect	0.81	88.42	600.35	4.38	569.78	6.24	20.07
Rank	7	3	1	6	2	5	4

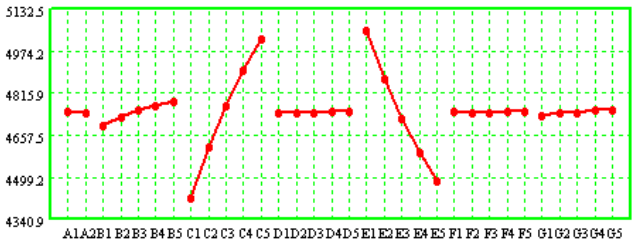

Fig.4 The response graphs

TABLE 4.
ANOVA

Factor	SS	DOF	Var	F	Confidence	Significance?	Rank
A	8.2898	1	8.2898		Pooled		7
B	49073.5	4	12268.4	249.953	100.00%	Yes	3
C	2235842	4	558960	11388.1	100.00%	Yes	1
D	141.334	4	35.3336		Pooled		6
E	2027210	4	506802	10325.4	100.00%	Yes	2
F	309.043	4	77.2608		Pooled		5
G	2703.65	4	675.911	13.7708	100.00%	Yes	4
Others	1161.07	24	48.3778		Pooled		
Error	1619.73	33	49.0828				
Total	4316449	49			At least 99% Confidence.		

6.2 Modeling and prediction of current density for a SOFC stack

The goal of the training process of BPNN is to realize the mapping relations between the inputs and the outputs by the training data. For the inputs, seven factors, as listed in Table 1 are considered. The only desired outputs in training data are the current densities for 10 layers in a SOFC stack which derive by the developed direct solution of Fortran program. Thus, the training data will be learned further to develop the model of the current density by the improved BPNN.

The training procedures are finished as the error converges steadily. Thus, the implemented neural network algorithm is used to predict testing data. Usually, the fact that the training procedures converges successfully can not always give the proof of excellent testing results. Therefore, it is noted that both superior learning results and testing results clarify the efficiency of the obtained model. To assess the accuracy of the learned model at all factor and level, all seven factors with variable levels are designed for the testing data, as listed in Table 5. Thus, Taguchi's orthogonal array $L_{18}(2^1x3^7)$ which columns from 1 to 7 are applied to design the testing data. Therefore, a total of 18 testing data for the learning of the network are adopted here.

By the processes of try and errors, it is found that 7 neurons in first hidden layer and 7 neurons in second hidden layer are more efficient for both better learning results and testing results. Therefore, 7×7×7×10 network structure is utilized here to perform the learning scheme. The learning results, including the array of factors and value of all levels, are listed in Table 5. Also, the testing results are listed in Table 6.

Compared with the direct solutions, the mean percent errors for the training results and the testing results are 0.117% and 0.231%, respectively. The small mean percent errors verify that the superior mapping relations between inputs and outputs can be realized by the improved BPNN with great satisfaction. Hence, the development of the model of the current density has been accomplished by the implemented neural network algorithm.

Thus, the accuracy and effectiveness of the developed BPN algorithm are certified. The results also show that the capability of fast calculation is very significant for the presented mathematical algorithm model than the FORTRAN program. Utilization of this developed BPNN model, as a set of inputs is given, its output result of current density can be obtained immediately even in real time, a result that affords a capability of dynamic control.

TABLE 5.
THE DESIGN OF TRAINING DATA FOR ALL FACTORS AND LEVELS BY $L_{50}(2^1\times5^{11})$ AND THEIR LEARNING RESULTS AT THE 7×7×7×10 NETWORK STRUCTURE

Exp.	A	B	C	D	E	F	G	*D 1	*D 2	*D 3	*D 4	*D 5	*D 6	*D 7	*D 8	*D 9	*D 10	Error%
1	1	1	1	1	1	1	1	4601.30	4657.23	4673.50	4680.75	4683.86	4681.74	4679.56	4674.50	4651.59	4584.93	0.092
2	1	1	2	2	2	2	2	4627.25	4682.45	4699.95	4706.53	4708.96	4708.10	4705.07	4700.10	4677.55	4610.77	0.061
3	1	1	3	3	3	3	3	4647.12	4701.80	4720.07	4726.16	4728.25	4728.33	4724.58	4719.70	4697.38	4630.58	0.073
4	1	1	4	4	4	4	4	4661.55	4715.86	4734.53	4740.32	4742.30	4743.04	4738.70	4733.92	4711.73	4644.97	0.088
5	1	1	5	5	5	5	5	4671.80	4725.84	4744.70	4750.29	4752.32	4753.52	4748.68	4744.02	4721.91	4655.19	0.082
6	1	2	1	2	3	4	5	4323.22	4381.06	4396.55	4403.78	4408.29	4407.52	4401.79	4399.76	4376.38	4305.78	0.170
7	1	2	2	3	4	5	1	4373.38	4429.06	4451.71	4456.77	4455.69	4457.79	4453.44	4448.82	4427.15	4355.46	0.195
8	1	2	3	4	5	1	2	4431.25	4486.46	4509.40	4514.38	4513.26	4515.14	4511.85	4505.55	4483.94	4413.76	0.082
9	1	2	4	5	1	2	3	5136.31	5189.26	5207.16	5212.04	5213.29	5213.40	5211.56	5205.21	5184.59	5119.94	0.032
10	1	2	5	1	2	3	4	5073.48	5126.19	5143.04	5148.33	5150.83	5151.57	5147.39	5142.97	5122.00	5056.85	0.067
11	1	3	1	3	5	2	4	4111.19	4169.98	4188.43	4194.32	4197.07	4199.18	4191.01	4190.45	4167.74	4092.31	0.054
12	1	3	2	4	1	3	5	4870.10	4925.24	4939.55	4946.86	4951.18	4947.62	4947.54	4940.28	4917.64	4854.64	0.226
13	1	3	3	5	2	4	1	4828.94	4883.27	4900.41	4906.79	4909.37	4907.76	4906.67	4899.43	4877.29	4813.08	0.248
14	1	3	4	1	3	5	2	4810.13	4864.00	4881.78	4887.66	4890.21	4889.78	4887.14	4880.68	4858.75	4794.04	0.338
15	1	3	5	2	4	1	3	4802.47	4856.14	4873.91	4879.80	4882.60	4882.71	4879.31	4873.15	4851.20	4786.26	0.306
16	1	4	1	4	2	5	3	4512.21	4571.08	4582.15	4591.08	4598.60	4592.11	4593.45	4584.93	4560.31	4497.39	0.130
17	1	4	2	5	3	1	4	4548.54	4605.92	4619.83	4627.83	4633.34	4629.14	4629.10	4621.16	4597.35	4533.11	0.238
18	1	4	3	1	4	2	5	4586.10	4642.15	4659.66	4666.14	4669.30	4667.01	4666.94	4657.66	4634.88	4570.49	0.041
19	1	4	4	2	5	3	1	4592.67	4647.59	4669.24	4674.36	4674.50	4674.16	4674.36	4663.88	4642.07	4576.69	0.038
20	1	4	5	3	1	4	2	5292.90	5345.67	5364.92	5368.19	5368.44	5369.50	5368.51	5360.45	5340.90	5276.49	0.224
21	1	5	1	5	4	3	2	4246.22	4307.37	4318.96	4327.44	4335.29	4329.64	4329.98	4321.60	4296.64	4230.81	0.062
22	1	5	2	1	5	4	3	4317.96	4376.02	4396.02	4401.87	4403.30	4401.57	4402.23	4392.00	4369.32	4301.64	0.125
23	1	5	3	2	1	5	4	5077.48	5131.41	5148.27	5153.81	5156.15	5153.82	5154.95	5145.52	5124.34	5061.96	0.030
24	1	5	4	3	2	1	5	5024.09	5077.58	5094.48	5100.25	5102.77	5101.64	5100.55	5093.09	5071.73	5008.14	0.034
25	1	5	5	4	3	2	1	4969.58	5022.64	5040.62	5046.21	5048.35	5048.22	5046.06	5039.02	5017.73	4953.38	0.021
26	2	1	1	1	4	5	4	4171.31	4227.39	4252.98	4256.91	4253.58	4259.23	4250.51	4250.41	4229.57	4151.30	0.091
27	2	1	2	2	5	1	5	4258.26	4313.63	4339.16	4343.25	4340.08	4345.07	4337.81	4335.75	4314.88	4238.89	0.089
28	2	1	3	3	1	2	1	4943.44	4996.87	5015.38	5020.99	5022.14	5021.46	5020.19	5013.35	4992.00	4927.28	0.094
29	2	1	4	4	2	3	2	4914.46	4967.73	4985.54	4991.28	4993.26	4993.36	4990.16	4984.88	4963.33	4898.09	0.038
30	2	1	5	5	3	4	3	4890.68	4943.85	4960.93	4966.81	4969.61	4970.31	4965.45	4961.54	4939.78	4874.13	0.042
31	2	2	1	2	1	3	3	4640.80	4697.31	4712.64	4720.18	4724.00	4720.01	4720.57	4712.76	4689.58	4625.26	0.212
32	2	2	2	3	2	4	4	4661.35	4716.91	4733.88	4740.62	4743.48	4741.25	4740.36	4733.17	4710.48	4645.48	0.133
33	2	2	3	4	3	5	5	4676.68	4731.55	4749.51	4755.69	4758.06	4757.17	4755.00	4748.43	4726.05	4660.57	0.059
34	2	2	4	5	4	1	1	4669.39	4723.64	4744.75	4750.05	4750.18	4750.45	4749.25	4740.82	4719.04	4653.19	0.049
35	2	2	5	1	5	2	2	4673.27	4727.23	4748.56	4753.49	4753.69	4754.59	4752.45	4744.57	4722.95	4656.97	0.168
36	2	3	1	3	3	1	2	4332.84	4391.45	4408.27	4415.37	4418.75	4415.96	4415.47	4407.83	4384.36	4316.54	0.246
37	2	3	2	4	4	2	3	4398.73	4455.65	4475.59	4481.62	4482.75	4481.84	4480.87	4472.83	4450.28	4382.10	0.265
38	2	3	3	5	5	3	4	4452.35	4508.09	4530.10	4535.36	4535.06	4535.39	4534.21	4525.66	4503.74	4435.59	0.133
39	2	3	4	1	1	4	5	5166.59	5219.52	5237.97	5242.39	5243.45	5243.31	5242.49	5234.64	5214.36	5150.37	0.112
40	2	3	5	2	2	5	1	5093.00	5145.59	5164.14	5168.93	5170.24	5170.71	5168.41	5161.78	5141.25	5076.53	0.067
41	2	4	1	4	5	4	1	4107.98	4167.03	4189.19	4194.07	4193.78	4195.15	4191.92	4185.82	4163.64	4089.86	0.184
42	2	4	2	5	1	5	2	4885.53	4940.64	4957.20	4963.90	4966.55	4962.47	4965.35	4954.68	4932.48	4870.48	0.191
43	2	4	3	1	2	1	3	4861.71	4916.18	4934.04	4940.16	4942.33	4939.74	4941.17	4930.99	4909.07	4846.34	0.121
44	2	4	4	2	3	2	4	4846.06	4900.03	4917.99	4923.91	4926.33	4925.07	4924.28	4915.79	4893.96	4830.29	0.070
45	2	4	5	3	4	3	5	4832.84	4886.46	4904.23	4910.08	4912.92	4912.63	4909.99	4902.97	4881.14	4816.77	0.072
46	2	5	1	5	2	2	5	4540.58	4600.39	4609.80	4619.48	4628.15	4619.20	4623.76	4612.26	4587.05	4526.74	0.103
47	2	5	2	1	3	3	1	4559.92	4617.29	4635.48	4642.10	4644.46	4639.54	4644.76	4630.46	4607.44	4545.36	0.041
48	2	5	3	2	4	4	2	4590.80	4646.89	4667.07	4672.85	4673.96	4671.07	4674.50	4661.23	4638.89	4575.69	0.046
49	2	5	4	3	5	5	3	4614.45	4669.64	4690.87	4696.12	4696.67	4695.27	4697.05	4684.88	4662.96	4598.93	0.062
50	2	5	5	4	1	1	4	5322.94	5375.82	5395.92	5398.80	5398.34	5399.31	5399.50	5390.15	5370.84	5306.66	0.114

*: BPN network output results

Ave: 0.117%

TABLE 6.
THE DESIGN OF TESTING DATA FOR ALL FACTORS AND LEVELS BY $L_{18}(2^1x3^7)$ AND THEIR TESTING RESULTS

Exp.	d_{stack}	N_f	X_{H_2}	X_{CO_2}	X_{H_2O}	X_{CO}	N_a	Ia1	Ia2	Ia3	Ia4	Ia5	Ia6	Ia7	Ia8	Ia9	Ia10	Error%
								*D 1	*D 2	*D 3	*D 4	*D 5	*D 6	*D 7	*D 8	*D 9	*D 10	
1	1	0.06	0.24	0.03	0.03	0.2	0.12	4602.28	4650.64	4669.90	4677.02	4679.25	4679.10	4676.38	4668.03	4645.64	4589.95	0.084
								4601.26	4656.81	4672.31	4679.02	4683.65	4681.34	4679.44	4674.48	4650.65	4583.67	
2	1	0.09	0.36	0.05	0.05	0.28	0.18	4645.11	4697.39	4716.29	4722.71	4724.62	4724.49	4722.13	4714.44	4691.98	4630.25	0.918
								4687.42	4742.35	4758.78	4764.74	4769.14	4767.46	4766.32	4758.98	4735.42	4670.36	
3	1	0.12	0.48	0.07	0.07	0.36	0.24	4668.24	4722.50	4740.96	4746.92	4748.61	4748.49	4746.36	4739.12	4716.84	4651.68	1.337
								4731.71	4785.94	4802.94	4808.41	4812.95	4812.26	4810.39	4802.47	4779.23	4714.63	
4	1	0.06	0.24	0.05	0.05	0.36	0.24	4301.11	4356.67	4375.55	4381.67	4383.41	4383.29	4381.10	4373.68	4350.87	4284.15	0.060
								4302.70	4358.88	4375.27	4381.41	4386.24	4387.19	4379.00	4380.13	4356.50	4283.10	
5	1	0.09	0.36	0.07	0.07	0.2	0.12	4448.43	4504.36	4524.24	4530.76	4532.59	4532.49	4530.27	4522.59	4499.22	4434.00	0.107
								4444.49	4499.67	4521.03	4525.80	4526.88	4527.19	4525.93	4518.06	4495.21	4426.43	
6	1	0.12	0.48	0.03	0.03	0.28	0.18	5325.70	5380.08	5396.91	5401.71	5402.92	5402.85	5401.38	5395.60	5375.39	5310.30	0.208
								5315.54	5368.50	5387.51	5389.78	5391.11	5392.78	5392.26	5383.13	5362.98	5297.61	
7	1	0.06	0.36	0.03	0.07	0.28	0.24	4420.08	4475.54	4494.43	4500.56	4502.28	4502.16	4499.97	4492.54	4469.74	4403.20	0.194
								4428.31	4482.42	4505.46	4509.50	4509.09	4512.02	4507.09	4503.20	4481.00	4409.10	
8	1	0.09	0.48	0.05	0.03	0.36	0.12	5277.11	5326.48	5344.55	5350.62	5352.36	5352.26	5350.16	5343.00	5321.82	5264.37	0.253
								5262.29	5315.06	5333.50	5336.37	5338.10	5339.80	5338.14	5330.58	5310.05	5244.23	
9	1	0.12	0.24	0.07	0.05	0.2	0.18	4376.72	4436.94	4455.03	4460.02	4461.24	4461.18	4459.69	4453.69	4431.97	4359.73	0.079
								4377.49	4437.52	4446.13	4455.11	4465.90	4457.87	4460.13	4451.17	4424.92	4361.73	
10	1.5	0.06	0.48	0.07	0.05	0.28	0.12	4885.04	4932.17	4951.14	4958.23	4960.46	4960.31	4957.58	4949.28	4927.18	4872.70	0.059
								4882.76	4935.88	4953.00	4958.16	4961.69	4962.65	4958.45	4953.91	4931.24	4864.95	
11	1.5	0.09	0.24	0.03	0.07	0.36	0.18	4109.14	4168.03	4187.65	4193.75	4195.40	4195.30	4193.26	4185.94	4162.43	4092.12	0.490
								4088.91	4145.41	4170.87	4173.89	4172.08	4175.97	4170.53	4167.34	4145.66	4068.36	
12	1.5	0.12	0.36	0.05	0.03	0.2	0.24	5078.23	5134.78	5151.36	5155.86	5156.94	5156.88	5155.55	5150.09	5129.89	5060.97	0.048
								5077.43	5131.33	5148.45	5153.25	5156.13	5154.14	5156.19	5145.77	5123.83	5060.50	
13	1.5	0.06	0.36	0.07	0.03	0.36	0.18	4961.83	5011.26	5029.42	5035.68	5037.55	5037.43	5035.11	5027.63	5006.05	4947.58	0.067
								4956.31	5009.77	5026.51	5031.74	5035.00	5034.57	5032.52	5026.67	5004.25	4938.71	
14	1.5	0.09	0.48	0.03	0.05	0.2	0.24	4950.15	5005.48	5023.09	5028.34	5029.72	5029.63	5027.92	5021.53	5000.14	4933.11	0.047
								4949.37	5002.41	5019.13	5024.22	5028.14	5028.60	5025.30	5019.53	4997.14	4931.66	
15	1.5	0.12	0.24	0.05	0.07	0.28	0.12	4126.15	4186.38	4206.12	4212.01	4213.56	4213.49	4211.62	4204.68	4181.38	4110.36	0.028
								4128.56	4188.05	4206.77	4212.00	4215.60	4212.89	4214.13	4204.40	4180.52	4110.88	
16	1.5	0.06	0.48	0.05	0.07	0.2	0.18	4662.06	4714.42	4733.51	4740.08	4742.03	4741.90	4739.48	4731.65	4708.93	4646.97	0.061
								4663.81	4717.58	4737.79	4742.33	4744.08	4745.31	4742.48	4735.81	4713.02	4646.15	
17	1.5	0.09	0.24	0.07	0.03	0.28	0.24	4686.80	4743.01	4760.78	4766.01	4767.38	4767.29	4765.60	4759.25	4737.66	4669.51	0.074
								4684.45	4741.30	4753.06	4761.05	4768.38	4762.39	4764.37	4755.91	4731.21	4668.24	
18	1.5	0.12	0.36	0.03	0.05	0.36	0.12	4716.73	4773.20	4792.09	4797.87	4799.41	4799.34	4797.50	4790.67	4768.37	4701.83	0.051
								4720.82	4775.93	4794.59	4799.90	4802.70	4799.71	4803.06	4790.53	4767.42	4704.56	

*: BPN network output results

Ave: 0.231%

6.3 Optimization of performance for a SOFC stack

As section mentioned above, the model of the average current density for each layer in a SOFC stack is developed by the improved BPNN. Thus, its calculating algorithms are applied to proceed with the optimization of the performance for a SOFC stack. The optimized procedures are finished as the objective function F, i.e. performance function converges to maximum or minimum. The results show that the Maximum F and the minimum F converge steadily to F_{max} =53907.89 and F_{min} =41137.11, respectively, no matter what random initial operating parameters, converging rate η^*, $0.01 \le \eta^* \le 0.3$, and momentum factor γ^*, $0.2 \le \gamma^* \le 0.8$, are selected. As illustrated in Fig.5, when the iteration T increases, the optimized processes are expected to converge steadily and quickly. Thus, operating performance window of a SOFC stack, $F_{min} \le F \le F_{max}$, is between 41137.11 and 53907.89.

As showed in Table 4, the significance factors are X_{H_2}, X_{H_2O}, N_f, N_a, respectively, whose responses all reveal linear relationship approximately. Therefore, in the consideration of the significance factors, it is reasonable that both the optimal operating parameters for the best performance, B_5 C_5 E_1 G_5, and the worst operating parameters for the worst performance, B_1 C_1 E_5 G_1, fall at boundary levers, as case 2 and 4 listed in Table 7. The optimal levels by the Taguchi method have the same selection of operating parameters for the significance factors, whose levels of the best performance are A_1 B_5 C_5 D_4 E_1 F_5 G_5 and levels of the worst performance are A_2 B_1 C_1 D_1 E_5 F_2 G_1, as case 1 and 3 listed in Table 7. The prediction of the best performance as well as the worst performance shows that the optimized method of the application of BPNN has better optimal results than Taguchi method.

Compared with the direct solution by FORTRAN program, all errors for the prediction of the performance of all cases listed in Table 7 are satisfactorily small. Hence, the calculating algorithms developed by the improved BPNN are proved to effectively obtain the optimized operating parameters.

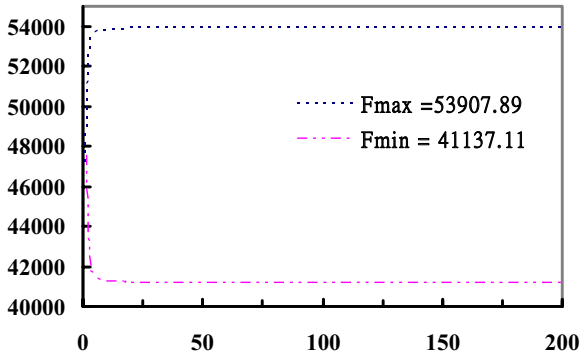

Fig.5 The converging process of optimization

6.4 Inverse prediction of operating parameters

The operating performance window of a SOFC stack studied here is $41137.11 \leq F \leq 53907.89$, as section mentioned above. Taking 5 desired performances as examples, the objective function converges steadily to the desired performance output Q in the optimized processes when the iteration T increases, as illustrated in Fig.6.

Compared with the direct solution by FORTRAN program, all errors for the prediction of the desired performance of all cases listed in Table 8 are satisfactorily small. Hence, the inverse prediction of operating parameters developed by the calculating algorithms of the improved BPNN shows great effectiveness in achieving a desired performance of a SOFC stack.

Instead of the direct solving procedure, the inverse calculating algorithm developed by the improved BPNN can provide a quick prediction of operating parameters to achieve a desired performance of a SOFC stack so as to complete dynamic control of the operating parameters,, such as the mole fraction of species and molar flow rate in inlet which are considered to be changeable.

It is noted that a desired performance usually has multi sets of solutions as the calculating algorithms of inverse prediction of operating parameters proceed. It is better to fix the levels for those operating parameters are insignificant factors, and then unite solution can be achieved by the adjustment of one significant operating parameter with fixed levels of the other significant factors. They are our future works.

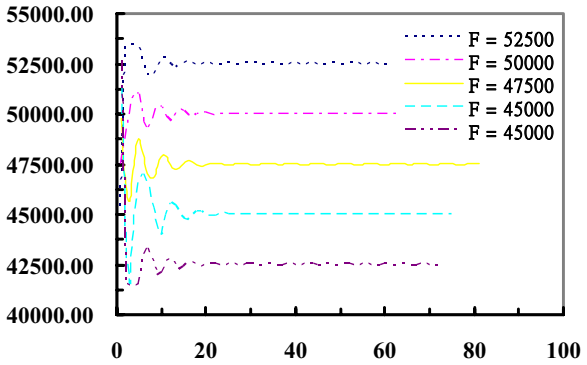

Fig.6 The converging process of inverse prediction of operating parameters for desired performances of a SOFC stack

TABLE 7.
PREDICTIONS OF MAXIMUM AND MINIMUM PERFORMANCE FOR A SOFC STACK.

No.	d_{stack}	N_f	X_{H_2}	X_{CO_2}	X_{H_2O}	X_{CO}	N_a	Ia1	Ia2	Ia3	Ia4	Ia5	Ia6	Ia7	Ia8	Ia9	Ia10	F	Error%
								*D 1	*D 2	*D 3	*D 4	*D 5	*D 6	*D 7	*D 8	*D 9	*D 10	*F	
1	1	0.12	0.48	0.06	0.03	0.36	0.24	5330.56	5385.83	5402.00	5406.39	5407.44	5407.39	5406.08	5400.74	5381.05	5313.86	53841.33	0.071
								5327.83	5380.94	5399.45	5401.72	5403.29	5405.04	5404.17	5395.55	5375.33	5309.89	53803.21	
2	1.5	0.12	0.48	0.03	0.03	0.36	0.24	5329.47	5384.39	5400.77	5405.29	5406.39	5406.33	5404.97	5399.48	5379.54	5312.64	53829.27	0.146
								5338.16	5391.17	5410.70	5412.57	5413.60	5415.25	5415.36	5405.34	5385.46	5320.29	53907.89	
3	1.5	0.06	0.24	0.03	0.07	0.24	0.12	4059.61	4112.15	4133.06	4140.81	4143.25	4143.09	4140.11	4131.02	4106.66	4045.84	41155.59	0.129
								4057.58	4112.33	4141.80	4143.52	4138.52	4146.46	4136.89	4137.72	4117.33	4035.24	41167.38	
4	1.5	0.06	0.24	0.0397	0.07	0.36	0.12	4059.48	4111.94	4132.86	4140.62	4143.06	4142.90	4139.93	4130.82	4106.45	4045.74	41153.8	0.135
								4054.50	4109.03	4139.22	4140.71	4135.09	4143.53	4133.63	4134.81	4114.63	4031.965	41137.11	

*: BPNN output results

TABLE 8.
THE INVERSE PREDICTION OF OPERATING PARAMETERS TO ACHIEVE A DESIRED PERFORMANCE OF A SOFC STACK FOR 5 EXAMPLES

No.	d_{stack}	N_f	X_{H_2}	X_{CO_2}	X_{H_2O}	X_{CO}	N_a	Ia1	Ia2	Ia3	Ia4	Ia5	Ia6	Ia7	Ia8	Ia9	Ia10	F	Error%
								*D 1	*D 2	*D 3	*D 4	*D 5	*D 6	*D 7	*D 8	*D 9	*D 10	*F	
1	1.2236	0.0983	0.4798	0.0491	0.0358	0.3089	0.2184	5176.78	5230.69	5247.71	5252.75	5254.07	5253.99	5252.35	5246.25	5225.72	5160.90	52301.21	0.378
								5197.47	5250.23	5267.86	5271.45	5273.95	5275.23	5273.07	5266.14	5245.12	5179.48	52500.00	
2	1.0887	0.0928	0.4768	0.06	0.0501	0.2316	0.2392	4938.45	4994.06	5011.40	5016.50	5017.82	5017.73	5016.08	5009.89	4988.88	4921.76	49932.57	0.134
								4946.87	5000.06	5016.10	5021.45	5025.77	5026.12	5022.50	5017.29	4994.69	4929.17	50000.00	
3	1.0492	0.1016	0.4136	0.0462	0.0595	0.3026	0.1546	4694.24	4750.35	4768.94	4774.67	4776.21	4776.12	4774.23	4767.42	4745.38	4679.19	47506.75	0.014
								4695.19	4749.68	4767.76	4773.07	4776.51	4775.56	4774.78	4766.24	4743.05	4678.15	47500.00	
4	1.07	0.06	0.3697	0.0357	0.0699	0.2094	0.1725	4428.41	4481.80	4501.19	4507.85	4509.82	4509.68	4507.24	4499.31	4476.34	4413.55	44835.19	0.366
								4443.48	4497.55	4521.31	4525.18	4524.20	4526.93	4523.19	4517.88	4495.77	4424.51	45000.00	
5	1.0539	0.06	0.2793	0.0416	0.07	0.2952	0.198	4199.68	4255.35	4275.00	4281.55	4283.45	4283.32	4280.95	4273.07	4249.59	4183.43	42565.39	0.153
								4192.29	4246.80	4271.70	4275.07	4273.55	4279.40	4269.70	4271.04	4249.57	4170.89	42500.00	

*: BPNN output results

VII. Conclusions

In this study, a model of average current densities for a SOFC stack is firstly established by the application of an improved back-propagation neural network. For the inputs of BPNN, the conditions of operating parameters are arranged by Taguchi's method with totally 7 factors. For the outputs of BPNN, the average current densities are achieved by the direct solution of numerical method. The results show that the presented model can effectively predict the performance of a SOFC stack with extremely small predicting errors less than 0.231%. According to the learning data, the analysis of variance reveals that the significance of all factors in order is molar fraction H_2 in anode inlet, molar fraction H_2O in anode inlet, mole flow rate in anode inlet, mole flow rate in cathode inlet, respectively.

Secondly, the mathematical algorithms developed by the improved BPNN are utilized to carry out the optimization of the performance of a SOFC stack. The operating performance window of a SOFC stack is derived by the optimized maximum and minimum performance function, which is $41137.11 \leq F \leq 53907.89$.

Similar to the optimized process, an inverse predicting model of operating parameters of a SOFC stack is developed by suitably adjusting the same calculating algorithms of the improved BPNN, where the object function based on the desired performance is suitably revised. The results show that, the inverse model can effectively predict operating parameters to obtain a desired performance output of a SOFC stack, whose scale is in the operating performance window.

Instead of the direct solving procedure by numerical method, all the calculating algorithms developed by the improved BPNN provide a series of interpretation on the applications of a SOFC stack: predict the performance of the average current density, evaluate the operating parameters of optimal performance and predict the conditions of operating parameters at a desired performance output. Combination of these calculating algorithms gives the possibility to complete dynamic control of the operating parameters, such as the mole fraction of species and molar flow rate in inlet which are considered to be changeable.

References

[1] Yakabe, H., Hishinuma, M., Uratani, M., Matsuzaki, Y., Yasuda, I., "Evaluation and modeling of performance of anode-supported solid oxide fuel cell", J. Power Sources, vol. 86, 2000, pp. 423-431.
[2] Yakabe, H., Ogiwara, T., Hishinuma, M., Yasuda, I., "3-D model calculation for planar SOFC", J. Power Sources, vol. 102, 2001, pp. 144-154.
[3] Recknagle, K.P., Williford, R.E., Chick, L.A., Rector, D.R., Khaleel, M.A., "Three-dimensional thermo-fluid electrochemical modeling of plannar SOFC stacks", J. Power Sources, vol. 113, 2003, pp. 109-114.
[4] Beale, S.B., Lin, Y., Zhubrin, S.V., Dong, W., "Computer methods for performance prediction in fuel cells", J. Power Sources, vol. 118, 2003, pp. 79-85.
[5] Iwata, M., Hikosaka, T., Morita, M., Iwanari, T., Ito, K., Onda, K., Esaki, Y., Sakaki, Y., Nagata, S., "Performance analysis of planar-type unit SOFC considering current and temperature distributions, Solid State Ionics", vol. 132, 2000, pp. 297-308.
[6] J.J. Huang, C.K. Chen and D.Y. Lai, J. Power Sources 140 (2005), pp. 235–242.
[7] V.M. Janardhanan, V. Heuveline and O. Deutschmann, J. Power Sources 172 (2007), pp. 296–307.
[8] T. Araki, T. Ohba, S. Takezawa, K. Onda and Y. Sakaki, J. Power Sources 158 (2006), pp. 52–59.
[9] H. Hirata and M. Hori, J. Power Sources 63 (1996), pp. 115–120.
[10] S.F. Liu, H.S. Chu and P. Yuan, J. Power Sources 161 (2006), pp. 1030–1040.
[11] P. Yuan and S.F. Liu, Numer. Heat Transf. A: Appl. 51 (2007), pp. 941–957
[12] P. Costamagna, E. Arato, E. Achenbach and U. Reus, J. Power Sources 52 (1994), pp. 243–249.
[13] R.J. Boersma and N.M. Sammes, J. Power Sources 66 (1997), pp. 41–45.
[14] T. Okada, S. Matsumoto, M. Matsumura, M. Miyazaki and M. Umeda, J. Power Sources 162 (2006), pp. 1029–1035.
[15] Ping Yuan, J. Power Sources 185 (2008), pp. 381-391.
[16] Arriagada, J., Olausson, P., Selimovic, A., "Artificial neural network simulator for SOFC performance prediction", J. Power Sources, vol. 112, 2002, pp. 54-60.
[17] J.H. Koh, H.K. Seo, Y.S. Yoo and H.C. Lim, Chem. Eng. J. 87 (2002), pp. 367–379.
[18] L.J.M.J. Blomen and M.N. Mugerwa, Fuel Cell Systems, Plenum Press, New York (1993) pp. 73–75.
[19] S.H. Chan, K.A. Khor and Z.T. Xia, J. Power Sources 93 (2001), pp. 130–140.
[20] J. Larminie and A. Dicks, Fuel Cell Systems Explained (1st ed.), Wiley, West Sussex (2000) p. 53.
[21] R. Maric, S. Ohara, T. Fukui, H. Yoshida, M. Nishimura, T. Inagaki and K. Miura, J. Electrochem. Soc. 146 (1999), pp. 2006–2010.
[22] A.L. Hines and R.N. Maddox, Mass Transfer Fundamentals and Applications, Prentice-Hall, New Jersey (1985) pp. 17–59.
[23] Wang, S.B., Wu, C.F., "Selections of working conditions for creep feed grinding. Part (III): avoidance of the work piece burning by using improved BP neural network", Int. J. Adv. Manuf. Technol., vol. 28, 2006, pp. 31-37.
[24] Rangwala, S., Dornfeld, D., "Learning and optimization of machining operations using computing abilities of neural networks", IEEE Trans. on Systems, man and Cybernetics', vol.19, No. 2, 1989, pp. 299-314.
[25] Peace, G., Taguchi Method: A Hands-on Approach, Addison-Wesley, Reading, MA,1993.